Controlled Growth of the Inorganic Backbone in Low-Dimensional Perovskites for Efficient, Stable, Semi-Transparent Wide Bandgap Perovskite Solar Cells

Andrea Zanetta
University of Pavia
Badri Vishal
King Abdullah University of Science and Technology
Fabiola Faini
University of Pavia
Giovanni Pica
University of Pavia
Sergio Marras
Istituto Italiano di Tecnologia
Bumin Yildirim
King Abdullah University of Science and Technology
Maxime Babics
King Abdullah University of Science and Technology
Esma Ugur
King Abdullah University of Science and Technology https://orcid.org/0000-0003-0070-334X
Erkan Aydin
King Abdullah University of Science and Technology https://orcid.org/0000-0002-8849-2788
Stefaan De Wolf
King Abdullah University of Science and Technology https://orcid.org/0000-0003-1619-9061
Michele De Bastiani
University of Pavia https://orcid.org/0000-0002-4870-2699
Giulia Grancini (✉ giulia.grancini@unipv.it)
University of Pavia https://orcid.org/0000-0001-8704-4222

Article

Keywords:

Posted Date: July 12th, 2023

DOI: https://doi.org/10.21203/rs.3.rs-2985134/v1

Additional Declarations: There is **NO** Competing Interest.

Controlled Growth of the Inorganic Backbone in Low-Dimensional Perovskites for Efficient, Stable, Semi-Transparent Wide Bandgap Perovskite Solar Cells

Andrea Zanetta[1], Badri Vishal[2], Fabiola Faini[1], Giovanni Pica[1], Sergio Marras[3], Bumin Yildirim[2], Maxime Babics[2], Esma Ugur[2], Erkan Aydin[2], Stefaan De Wolf[2], Michele De Bastiani[1], Giulia Grancini[1,]*

[1]Università Degli Studi Di Pavia - Pavia (Italy), Department of Chemistry & INSTM, Via T. Taramelli 14, 27100 Pavia, Italy

[2]King Abdullah University of Science and Technology (KAUST), KAUST Solar Center (KSC), Physical Sciences and Engineering Division (PSE), Thuwal, 23955-6900, Kingdom of Saudi Arabia

[3]Center for Convergent Technologies, Istituto Italiano di Tecnologia, Via Morego 30, 16163 Genova, Italy

**Corresponding author:* giulia.grancini@unipv.it

Abstract

Wide bandgap (WB) perovskites are of interest for envisioned applications in coloured and semi-transparent solar cells. For this, low dimensional perovskites (LDP) are of promise as they pair a wide bandgap with stability. However, so far, the power conversion efficiency (PCE) of LDP solar cells barely touched a few percentages, mainly due to inefficient charge transport. To overcome such limit is essential to control the growth of the crystalline backbone, which is dictated by the alignment of the inorganic planes. Here, we demonstrate an effective strategy, based on the judicious choice of additives and controlled seed growth in the perovskite solution, to guide the crystallization of LDPs inorganic layers perpendicularly to the substrate. The vertically aligned LDP solar cells (with a bandgap of 2.0 eV, n = 2) outperformed their non-oriented 2D counterpart, boosting the PCE to a

record value of 9.4 %. Furthermore, this sets a benchmark for the stability of WB PSCs, where 80% of the initial performance was retained after ~100 h illumination. To broaden the scope of our method, we fabricated semi-transparent LDP devices (transmittance > 30%) with a PCE of 6 % paving the way for the development of tuneable smart solar devices.

Introduction

Low-dimensional perovskites (LDP) show a layered structure, where organic and inorganic layers alternate[1,2]. The inorganic backbone is composed by stacking *n* layers of perovskite octahedra, spaced by organic cations, *n* defining the dimensionality of the LDP[3,4]. Compared to the well-known three-dimensional (3D) halide perovskites, LDPs offer a higher resilience to degradation and wider band gaps, thanks to the confinement effect which rules its layered crystalline structure[5–8]. So far, LDPs have been mainly implemented as interface modifiers in perovskite solar cells (PSCs), leading to the highest power conversion efficiencies (PCEs) reported so far thanks to a combined enhancement of charge extraction and stability [6,9–11]. On the other side, LDPs used *alone* as active layer show limited performances with PCE < 2 % for $n < 2$,[12] due to the preferential parallel-to-the-substrate growth of inorganic layer[13–15] that hinders the vertical charge transport in the device[2,16–19]. In order to address this constraint, we demonstrate a rational growth and crystal orientation of phase pure $n = 2$ LDPs, by using a strategy based on perovskite's seeds growth in the precursor solution and enhanced crystallization kinetics through methylammonium chloride (MACl) additive. Such control over the crystalline orientation, boosts the perovskite solar cell (PSC) performances, achieving a record PCE of 9.4 %. The vertically oriented LDP with a 2.0 eV band gap outperformed by more than 1000 % the reference, consisting of the common horizontally aligned material. Importantly, while the standard PSCs - based on common 3D perovskite - with similar band gap suffer from poor stability under illumination due to severe halide segregation,[20,21] our vertically aligned LDP device retains more than 80 % of its initial performance (T_{80}) after ~ 100 h under continuous illumination. Lastly, we show the versatility of our approach by fabricating semi-transparent devices with an average visible

transmittance (AVT) higher than 30 % and a PCE of 6 %, resulting in a light utilization factor (LUE) of about 1.86 %. Overall, our results break the current limits in the use of LDPs in high technological impact optoelectronics, ranging from WB photovoltaic devices for semi-transparent applications into smart buildings and greenhouses to optical and photonic devices.

75 **Main**

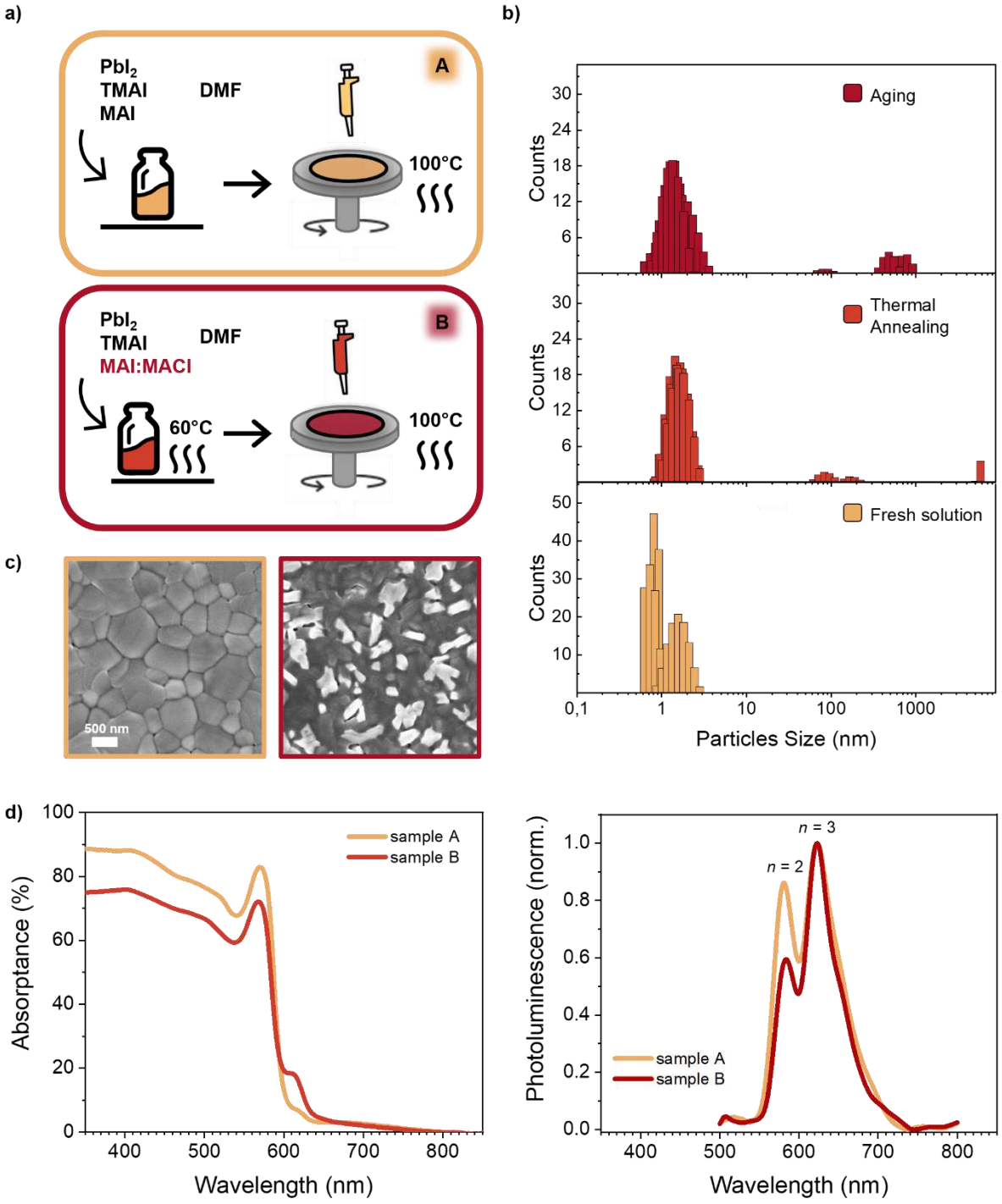

Figure 1. a) *Sketch representing the two experimental approaches for preparing LDP thin films.* ***b)*** *Results of the dynamic light scattering measurements performed on the LDP precursor solutions as prepared (fresh solution), after annealing or ageing treatment.* ***c)*** *SEM morphologic analysis on LDP thin film processed through process A (left) and process B (right).* ***d)*** *Optical analysis of samples A and B: UV-Vis light absorption (left) and photoluminescence (right).*

76

Figure 1 shows the experimental approach to prepare the LDP with chemical formula $TMA_2MAPb_2I_7$ ($R_nA_{n-1}Pb_nX_{2n+1}$) where R is thiophene methylammonium (TMA), A is methylammonium (MA), and X is iodide (I). We show two different experimental approaches for the preparation of the LDP: *i)* process (A) consists of the dissolution of the precursor powders in the stochiometric ratio in dimethylformamide (DMF) solvent and the successive spin coating and annealing steps (the details are described in supporting information - SI), a standard protocol which is commonly used in literature;[14,15,22] *ii)* process (B) is optimized by substituting 70 % of the methylammonium iodide (MAI) content in the solution with the MACl. In addition, the resulting precursor solution is annealed at 60° C for 2 h, before deposition, following the steps identical to process (A). On the one hand, the addition of MACl in the solution helps in increasing the kinetics of crystallization during the deposition process[23–25]. On the other hand, the thermal annealing of the precursor solution facilitates the nucleation of clusters inside of it, which plays a role during the crystallization of the thin film regulating the orientation of the crystals[26–28]. Figure 1b shows dynamic light scattering (DLS) measurement results, which gives insight about the nucleation of the clusters inside the solutions. We tested a freshly prepared solution, a thermally annealed one (60° C for 2 h), and an aged solution that has been left in an N_2 atmosphere at room temperature for 5 weeks. We note that in all three cases, the biggest fraction of particles is in the 1-4 nm diameter range, which is linked to the dissolved precursors of the perovskite. However, in the cases of thermal annealed and aged solutions, a relevant fraction of particles start to appear in the 100 nm range, which demonstrates the formation of perovskite clusters upon aging or thermal treatment.

Figure 1c shows the morphology of the LDP thin films prepared by following the two different processes by scanning electron microscopy (SEM). The two samples are significantly different in the two cases: the sample prepared with process A (sample A in the following) presents a continuous surface covered by large and flat crystals, whereas, in the case of process B (sample B), the material shows an indented surface with small crystals and strong contrasts. However, despite the different morphology, the optical properties of the two materials are preserved (see Figure 1d). The optical

absorption presents the features typical of two different LDP phases: a predominant $n = 2$ with a strong excitonic peak at 570 nm, and a second minor $n = 3$ phase with an excitonic peak at 615 nm. This indicates that the modifications in the processing do not affect the purity of the perovskite phase. We estimate the bandgap of the material from Tauc's plot interpolation for a direct semiconductor (Figure S2), deriving a bandgap of 2.0 eV. Photoluminescence (PL) spectra presents two emission peaks centered at 580 nm and 630 nm ascribable to the $n = 2$ and $n = 3$ LDP phases, which dominate due to energy transfer happening from low to high n phases[29,30].

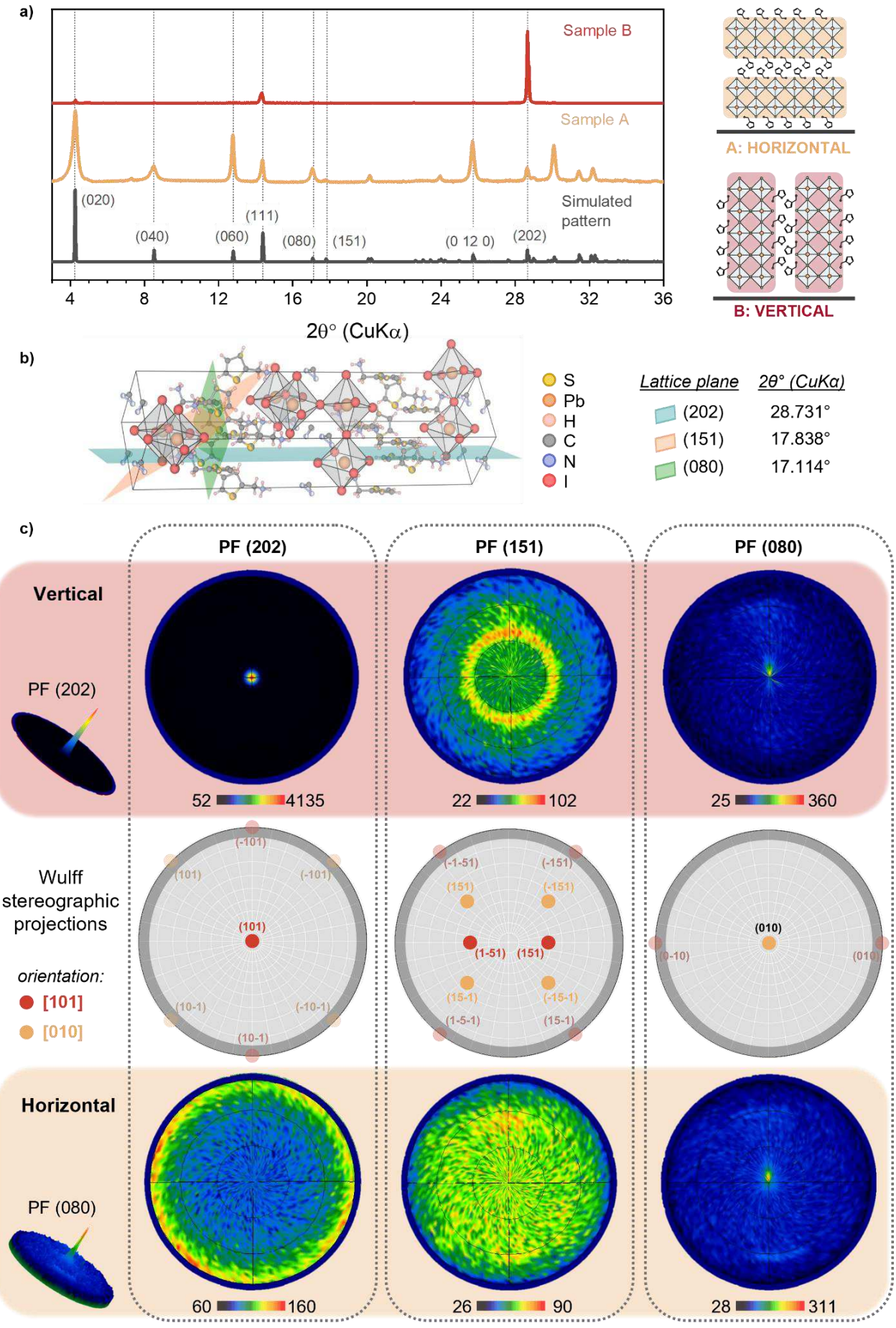
a)
Sample B
Sample A
Simulated pattern
(020)
(040)
(060)
(111)
(080)
(151)
(0 12 0)
(202)
4
8
12
16
20
24
28
32
36
2θ° (CuKα)
A: HORIZONTAL
B: VERTICAL
b)
S
Pb
H
C
N
I
Lattice plane
2θ° (CuKα)
(202)
28.731°
(151)
17.838°
(080)
17.114°
c)
PF (202)
PF (151)
PF (080)
Vertical
PF (202)
52
4135
22
102
25
360
Wulff stereographic projections
orientation:
[101]
[010]
(-101)
(101)
(-101)
(101)
(10-1)
(-10-1)
(10-1)
(-1-51)
(-151)
(151)
(-151)
(1-51)
(151)
(15-1)
(-15-1)
(1-5-1)
(15-1)
(010)
(0-10)
(010)
Horizontal
PF (080)
60
160
26
90
28
311

112

Figure 2. *X-Ray diffraction studies on the differently oriented LDP thin films.* ***a)*** *On the left, experimental XRD pattern for sample A and sample B and simulated pattern calculated from single crystal data reported in the literature. On the right, the cartoon depicts the two different crystalline orientations of the samples in which the inorganic perovskite octahedra n = 2 layers are oriented parallel/perpendicular to the substrate for the case of the horizontal/vertical sample.* ***b)*** *Representation of the unit cell for the* $TMA_2MAPb_2I_7$ *n = 2 LDP in which the different families of planes have been depicted with different colours (the lattice planes corresponding to the (101), (151), and (010) are represented in blue, red, and green respectively). The legend reports the family of planes considered for the further analysis and the 2theta angles at which their X-Ray reflection is detectable.* ***c)*** *Pole Figure images and Wulff stereographic projection for the different conditions considered. Pole figure images for the vertical and horizontal samples have been taken at different incident angles corresponding to the diffraction of the different families of planes. The outer dark grey ring in the calculated projection indicates a prohibited range for the experimental setup coinciding with the maximum sample tilt chi = 85°, so that the point within this area cannot be detected during the experiment.*

The structural properties in terms of X-Ray Diffraction (XRD) analysis are presented in Figure 2. Figure 2a shows the experimental XRD patterns for sample A and sample B, compared with the simulated pattern created with CrystalDiffract from the single crystal LDP structure reported in the literature[31]. The results are strikingly different: the relative intensities of peaks of sample A are very close to those of the simulated one, with a slightly higher intensity for the (0k0) peaks. Differently, in the pattern of sample B, the huge intensity of the (202) peak at 2θ values of 28.78° (CuKα) hinders most of the peaks except those at 4.23° and 14.32°, associated with (020) and (111) respectively. Also, no signals coming from $n = 3$ LDP impurities is detected, suggesting that in both samples the volume of the $n = 3$ phase is minor. From these results, we can assert that the two samples crystallize in two very different ways, in particular in the case of sample B the material spontaneously tends to grow with a strong preferential orientation as indicated by the overwhelming intensity of the (202) peak. Such an orientation coincides with a preferential vertical orientation of the inorganic sheets of the LDP with respect to the substrate. Contrarily, sample A orients preferentially with the inorganic planes arranged parallelly to the substrate, as represented in the cartoon (Fig.2a). Such results demonstrate that a fine adjustment in the crystallization process takes place and successfully reshapes the crystalline properties of the material. Figure 2b depicts the retrieved unit cell of the LDP. By looking at the unit cell, we note that by changing the preferential growth plane, the thin film exposes its inorganic planes, containing the PbI_6^- octahedra, oriented in a different direction with respect to the

substrate. Thus, when the [101] (or [010]) crystalline direction dominates, the preferred orientation of the LDP's inorganic backbone is vertical (or horizontal).

Figure 2c shows the results of the texture analysis we performed through XRD Pole Figure (PF) measurements. This technique is based on the acquisition of XRD data by varying the incidence angle along two different axes to build PF maps. In such way, it allows one to prove the different orientations of thin film crystalline samples by comparing them with the Wulff stereographic projection (WSP) calculated from single crystal data. Indeed, WSP predicts the PF images for a single crystal perfectly aligned along the [101] (in red) or [010] (in yellow) crystallographic direction. By comparing them with the PFs experimental data for the two samples, the vertical (sample B) and horizontal (sample A) ones, it is possible to understand the preferential orientation of the crystals in the thin film. We investigate the orientation of three different lattice planes (the same as those shown in Figure 2b): the (202), (151), and (080) that correspond to reflection at 28.73°, 17.83°, and 17.11° respectively. The strong peak at the centre of PF (202) confirms such preferential growth of the vertical sample along the [101] direction in which crystals tend to grow with a fibre-textured disposition as suggested by the ring observed in the PF (151) corresponding to the tilted plane reflections. Conversely, in the case of the horizontal sample, the PF (202) presents higher intensity in the outer ring coinciding with the diffraction of the (101) family of planes. Those are the responsible for the central peak of PF (080), confirming that in the horizontal sample the orientation is less prevailing, and a random disposition is more likely to take place.

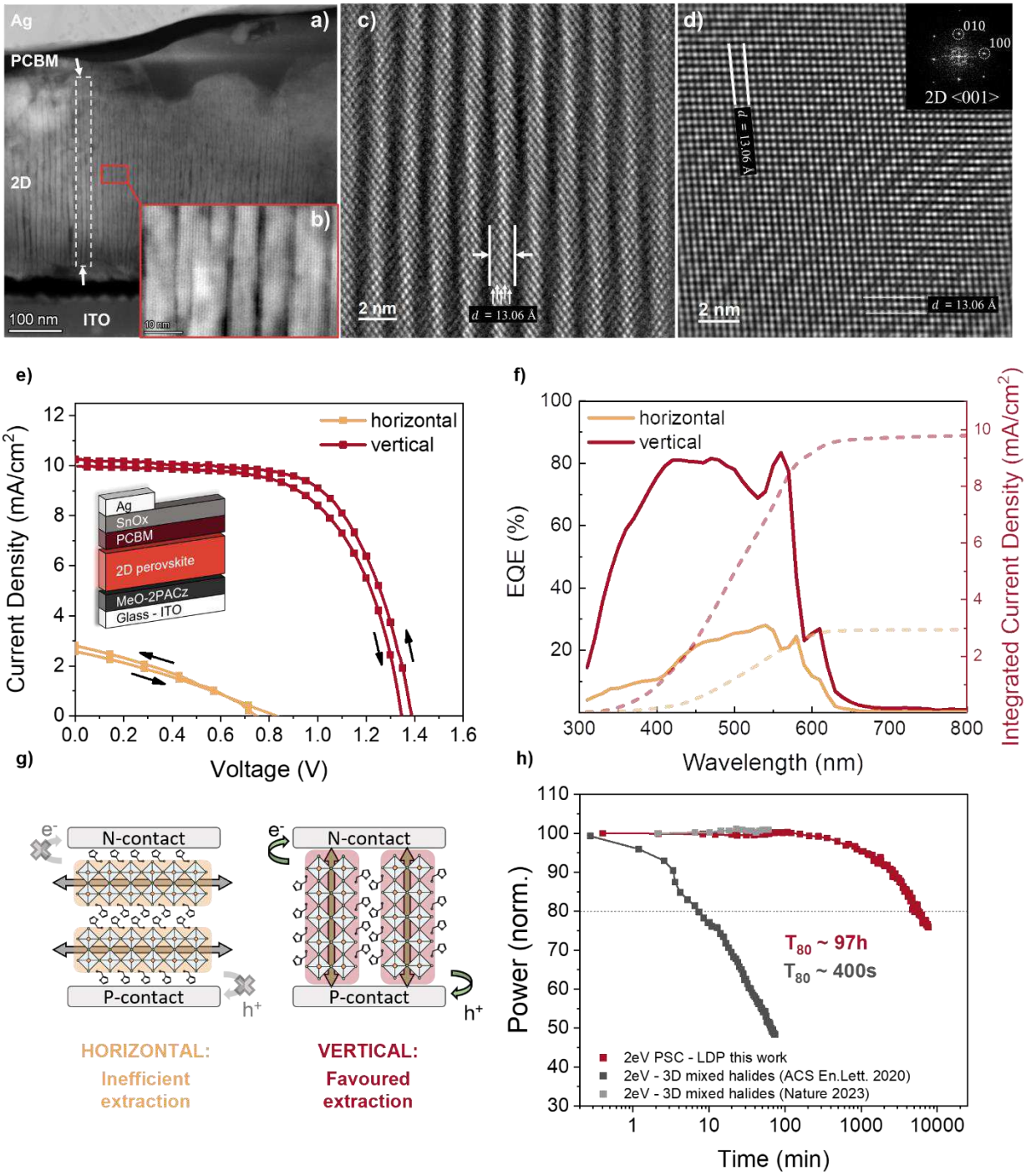

Figure 3. a-d) *TEM analysis on the structure of vertical LDP:* ***a)*** *large area cross-sectional HAADF-S-TEM image and* ***b)*** *HR-HAADF-STEM of the full device, showing large vertical grains.* ***c)*** *HR-TEM of a single inorganic stack of n = 2 LDP, with a dimension about 13.06 Å, separated by organic layers. White arrows represent 5 atoms stacks that compose the inorganic layer of the material.* ***d)*** *HR-TEM and corresponding FFT (insert) of LDP along zone axis <001>, confirming the lattice parameter of the material (a = b = 7.36 Å).* ***e)*** *Voltage-Current density curves (reverse and forward scan) for the PSC devices in which the horizontal/vertical LDP stands as a photoactive layer. The inset shows the stack of the device under investigation.* ***f)*** *External quantum efficiency and integrated current density for the horizontal and vertical devices.* ***g)*** *The sketch represents how the LDP is oriented within the device in the case of the horizontal/vertical device, inhibiting/favouring the extraction of charge carriers towards the external electrodes.* ***h)*** *Maximum power point tracking for three different 2.0 eV WB single-junction perovskite solar cells plotted on a logarithmic time axis. The red curve shows the experimental results for the stability of the LDP-based solar cell presented in this work (full data on SI). The data of the other two curves, related to 3D perovskite-based WB devices, have been reproduced from the literature (ref. 20 and 33).*

151

Furthermore, to visualize the alignment of the LDP, we perform a transmission electron microscopy (TEM) analysis on the cross-section of the vertical sample. The high-angle annular dark-field scanning TEM (HAADF-S-TEM) images are depicted in Figure 3a-d in a prototype device configuration based on ITO/MeO-2PACz/LDP/PCBM/SnO_X/Ag architecture. From the cross-section images, all the different layers composing the device stack are recognizable (elemental mapping is given in Fig. S5). The LDP layer is composed of large vertical grains that have followed a preferential columnar growth, aligned perpendicular to the ITO substrate with a length in the order of 300 nm, as much as the total thickness of the layer. By enhancing the magnification (Fig.3b), it is possible to observe the lack of grain boundary in the vertical direction, which makes charge transport within grains easier. Further increasing the resolution through the high-resolution TEM (HR-TEM) technique (Fig.3c-d), we observe that the features in the LDP layer correspond to the perpendicular alignment of the inorganic planes, in agreement with XRD. Indeed, in Figure 3c the vertical features can be ascribed to the layered structure of the LDP, in which the bright lines represent the inorganic sheet of the material with a spacing of about 13.06 Å that corresponds to the stack of two PbI_6^- octahedra layers, as for the case of an n = 2 LDP. Furthermore, Figure 3d shows HR-TEM and corresponding First Fourier Transform (FFT) along zone axis <001>, confirming that the lattice parameter of the material corresponds to a = b = 7.36 Å and that the n = 2 dimensionality of the perovskite in its RP phase (Fig.3d)[32].

To fully exploit the potential of a controlled crystalline orientation, we fabricate PSCs in the inverted configuration. Figure 3e shows the characteristic J-V curves for the devices based on the horizontal and vertical LDP (statistical distribution is presented in Fig.S3). The horizontal sample shows PCE around 0.8 %, strongly limited in its performances from the low short circuit current density (Jsc), in agreement with the literature[15,18]. Differently, the vertically oriented sample shows a best PCE of 9.4 %, with J_{SC} = 10.6 mA/cm^2, a fill factor (FF) of 63.2 %, and an open circuit voltage (V_{OC}) of 1.40 V which is, to the best of our knowledge, the highest reported so far for a device based on LDP with $n \leq 2$ (see Table S1 as reference).

To deeply investigate the difference in performances between the horizontal and vertical devices, we perform external quantum efficiency (EQE) measurements (Figure 3f). From the data, we note that the orientation of the LDP phase strongly affects the performances in terms of photogenerated current. However, at lower wavelengths, the EQE signal is significantly different for the two samples. The vertical sample achieves values of EQE higher than 80 % whereas the horizontal sample barely overcomes 25 % over the spectrum. Such a behaviour could be associated with a difference in the charge carriers' transport within the two devices, mainly related to the different alignment. Indeed, as schematically depicted in Figure 3g, in the case of the vertical device, the extraction of carriers is maximized since the alignment of the inorganic planes favours the transport towards the two electrodes. Additionally, the stability at its maximum power point (MPP) under continuous illumination has been tested. The vertical device shows a T_{80}, determined as the time necessary to reach 80% of its initial efficiency, of about 97 h. This results into a high stability, as visualized in Figure 3h (further stability data are reported in Figure S5) in which we compared our device with the best 2.0 eV PSC based on 3D perovskite reported in the literature so far[20,33]. Such behaviour can be associated with a different degradation mechanism occurring in the vertically aligned LDP encompassing the traditional instability limits of the 3D counterpart related to the intermixing of halide anions, which leads to halide segregation under illumination. In our case, no halide segregation happens (see also PL stability measurements Figure S8): the LDPs allow reaching a wide bandgap (≥ 2.0 eV) with pure iodine composition, reducing instability issues, and ultimately extending the lifetime of the devices. To verify the broad applicability of our method we also verify the orientation using mixed I/Br LDP formulations. Our findings indicate that the incorporation of Br alters the bandgap of the material, thus enabling colour and transparency modulation in devices with varying ratios of halides and demonstrating potential of such LDPs also for ultra-wide bandgap applications (Figure S7).

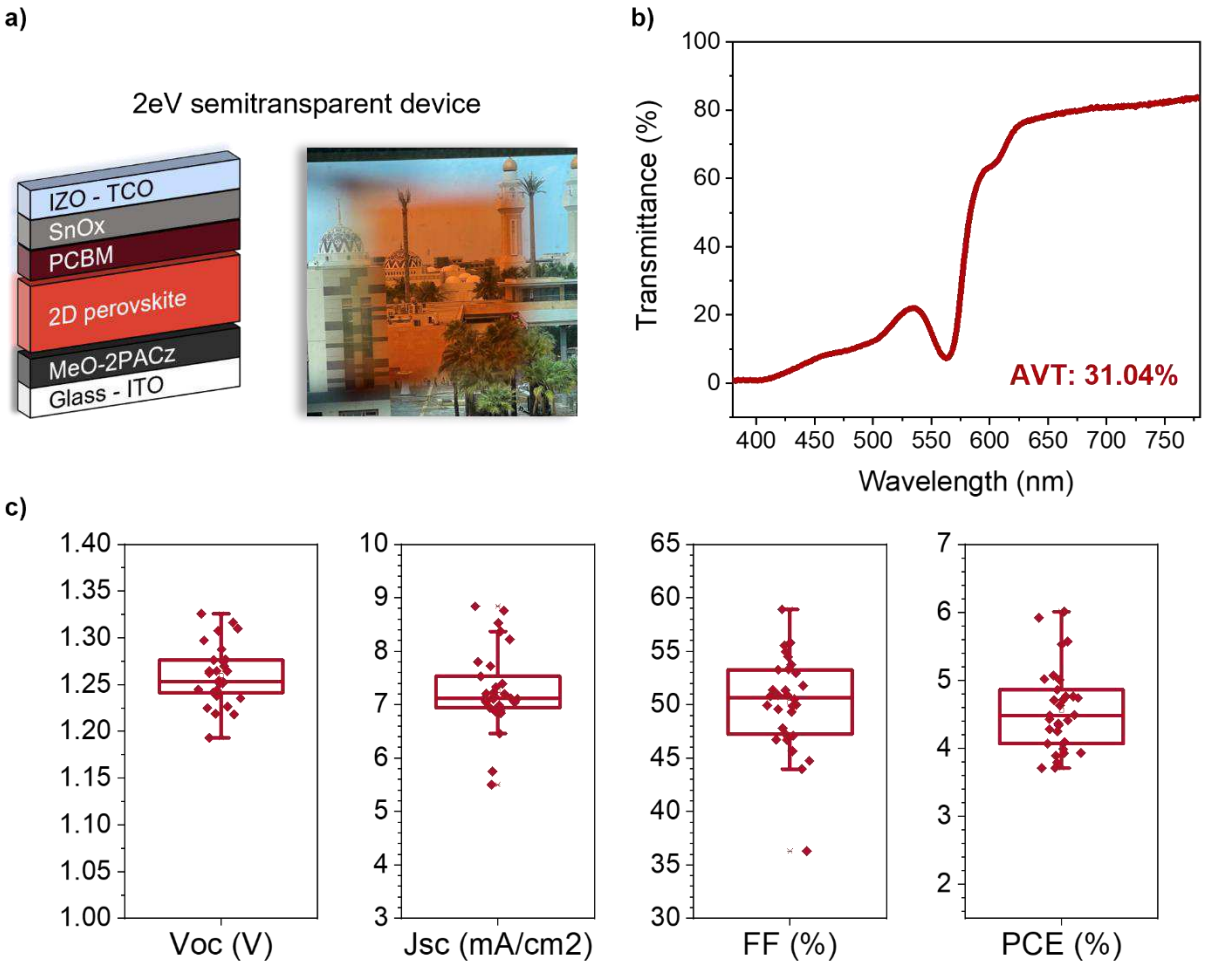

Figure 4. *Semi-transparent WB solar cell based on LDP material.* ***a)*** *Device stack and picture of the device showing the characteristic red colour and transparency.* ***b)*** *Light transmittance of the full device from which AVT has been calculated.* ***c)*** *Box charts reporting the performances of the semi-transparent devices over a batch of 25 solar cells in terms of V_{OC}, J_{SC}, FF and PCE.*

The vertical aligned LDP has been also tested in semi-transparent PSCs substituting the opaque Ag electrode with the Indium Zinc Oxide (IZO) transparent electrode, as shown in Figure 4a. The light transmission analysis, represented in Figure 4b, shows the high transmittance of the device that reaches values higher than 80 % in the region > 620 nm, resulting in a calculated AVT (see SI for details) of the device of 31 %, which meets the requirements for window-integrated photovoltaic applications. Concerning the performances (Figure 4c), the devices exhibit a consistent V_{OC} of about 1.30 V and a PCE of 6 %, resulting in an LUE of 1.86 %, in accordance with semi-transparent devices based on 3D perovskites reported in the literature.[34,35]

Conclusions

We demonstrate an effective strategy to control the crystal orientation of 2.0 eV LDPs and their successful implementation in solar cells. We established a method which forces the vertical alignment of the inorganic backbone of LDP with $n = 2$ dimensionality, essential for maximizing the charge extraction in photovoltaic devices. Through this method, we obtain 2.0 eV WB stable devices with PCE higher than 9 %, the highest reported so far among PSCs based on $n \leq 2$ LDPs. With such progress, WB perovskite absorbers become a viable opportunity for stable and efficient triple junction concepts. In this direction, we demonstrate that such vertically aligned materials can be effectively integrated into semi-transparent devices with a high grade of transparency (AVT 31 %), a PCE of 6 % and LUE of 1.86 %. Our approach can open new applications for LDPs, representing a new frontier material for building-integrated photovoltaics, smart windows, agri-photovoltaics and multijunction devices.

References

1. Grancini, G. & Nazeeruddin, M. K. Dimensional tailoring of hybrid perovskites for photovoltaics. *Nat Rev Mater* **4**, 4–22 (2019).
2. Xu, Y., Wang, M., Lei, Y., Ci, Z. & Jin, Z. Crystallization Kinetics in 2D Perovskite Solar Cells. *Advanced Energy Materials* **10**, 2002558 (2020).
3. Kim, E.-B., Akhtar, M. S., Shin, H.-S., Ameen, S. & Nazeeruddin, M. K. A review on two-dimensional (2D) and 2D-3D multidimensional perovskite solar cells: Perovskites structures, stability, and photovoltaic performances. *Journal of Photochemistry and Photobiology C: Photochemistry Reviews* **48**, 100405 (2021).
4. Chen, Y. *et al.* 2D Ruddlesden–Popper Perovskites for Optoelectronics. *Advanced Materials* **30**, 1703487 (2018).

5. Grancini, G. *et al.* One-Year stable perovskite solar cells by 2D/3D interface engineering. *Nat Commun* **8**, 15684 (2017).
6. Azmi, R. *et al.* Damp heat–stable perovskite solar cells with tailored-dimensionality 2D/3D heterojunctions. *Science* **376**, 73–77 (2022).
7. Sutanto, A. A. *et al.* In Situ Analysis Reveals the Role of 2D Perovskite in Preventing Thermal-Induced Degradation in 2D/3D Perovskite Interfaces. *Nano Lett.* **20**, 3992–3998 (2020).
8. Mahal, E., Mandal, S. C. & Pathak, B. Understanding the role of spacer cation in 2D layered halide perovskites to achieve stable perovskite solar cells. *Mater. Adv.* 10.1039.D1MA01135A (2022) doi:10.1039/D1MA01135A.
9. Degani, M. *et al.* 23.7% Efficient inverted perovskite solar cells by dual interfacial modification. *Science Advances* **7**, eabj7930 (2021).
10. Sutanto, A. A. *et al.* Dynamical evolution of the 2D/3D interface: a hidden driver behind perovskite solar cell instability. *J. Mater. Chem. A* **8**, 2343–2348 (2020).
11. Sutanto, A. A. *et al.* 2D/3D perovskite engineering eliminates interfacial recombination losses in hybrid perovskite solar cells. *Chem* S2451929421002035 (2021) doi:10.1016/j.chempr.2021.04.002.
12. Liang, C. *et al.* Two-dimensional Ruddlesden–Popper layered perovskite solar cells based on phase-pure thin films. *Nat Energy* (2020) doi:10.1038/s41560-020-00721-5.
13. Ji, T. *et al.* Crystallization regulation of solution-processed two-dimensional perovskite solar cells. *J. Mater. Chem. A* **10**, 13625–13650 (2022).
14. Li, Y., Zhao, Y., Cheng, H., Zhao, K. & Wang, Z.-S. Highly Efficient and Stable Pure Two-Dimensional Perovskite-Based Solar Cells with the 3-Aminopropionitrile Organic Cation. *ACS Appl. Mater. Interfaces* **12**, 18590–18595 (2020).
15. Liang, C. *et al.* Two-dimensional Ruddlesden–Popper layered perovskite solar cells based on phase-pure thin films. *Nat Energy* **6**, 38–45 (2021).

16. He, X. *et al.* Oriented Growth of Ultrathin Single Crystals of 2D Ruddlesden− Popper Hybrid Lead Iodide Perovskites for High-Performance Photodetectors. *ACS Appl. Mater. Interfaces* 8 (2019).
17. Yang, R. *et al.* Oriented Quasi-2D Perovskites for High Performance Optoelectronic Devices. *Adv. Mater.* **30**, 1804771 (2018).
18. Zhang, X. *et al.* Orientation Regulation of Phenylethylammonium Cation Based 2D Perovskite Solar Cell with Efficiency Higher Than 11%. *Advanced Energy Materials* **8**, 1702498 (2018).
19. J. Magdaleno, A. *et al.* Efficient interlayer exciton transport in two-dimensional metal-halide perovskites. *Materials Horizons* **8**, 639–644 (2021).
20. Xiao, K. *et al.* Solution-Processed Monolithic All-Perovskite Triple-Junction Solar Cells with Efficiency Exceeding 20%. *ACS Energy Lett.* **5**, 2819–2826 (2020).
21. Peña-Camargo, F. *et al.* Halide Segregation versus Interfacial Recombination in Bromide-Rich Wide-Gap Perovskite Solar Cells. *ACS Energy Lett.* **5**, 2728–2736 (2020).
22. Zanetta, A. *et al.* Manipulating Color Emission in 2D Hybrid Perovskites by Fine Tuning Halide Segregation: A Transparent Green Emitter. *Advanced Materials* **34**, 2105942 (2022).
23. Lai, H. *et al.* Two-Dimensional Ruddlesden–Popper Perovskite with Nanorod-like Morphology for Solar Cells with Efficiency Exceeding 15%. *J. Am. Chem. Soc.* **140**, 11639–11646 (2018).
24. Larini, V. *et al.* From Bulk to Surface Passivation: Double Role of Chlorine-Doping for Boosting Efficiency of FAPbI3-rich Perovskite Solar Cells. *Solar RRL* **6**, 2200038 (2022).
25. Kim, M. *et al.* Methylammonium Chloride Induces Intermediate Phase Stabilization for Efficient Perovskite Solar Cells. *Joule* **3**, 2179–2192 (2019).
26. Li, X. *et al.* Efficient and Stable Quasi-2D Perovskite Solar Cells Enabled by Thermal-Aged Precursor Solution. *Advanced Functional Materials* **n/a**, 2107675.
27. Lian, X. *et al.* The Second Spacer Cation Assisted Growth of a 2D Perovskite Film with Oriented Large Grain for Highly Efficient and Stable Solar Cells. *Angewandte Chemie International Edition* **58**, 9409–9413 (2019).

28. Luo, C. *et al.* Facet orientation tailoring via 2D-seed- induced growth enables highly efficient and stable perovskite solar cells. *Joule* **6**, 240–257 (2022).
29. Tsai, H. *et al.* Design principles for electronic charge transport in solution-processed vertically stacked 2D perovskite quantum wells. *Nat Commun* **9**, 2130 (2018).
30. Williams, O. F. *et al.* Energy transfer mechanisms in layered 2D perovskites. *The Journal of Chemical Physics* **148**, 134706 (2018).
31. Zhu, X.-H., Mercier, N., Riou, A., Blanchard, P. & Frère, P. (C4H3SCH2NH3)2(CH3NH3)Pb2I7 : non-centrosymmetrical crystal structure of a bilayer hybrid perovskite. *Chem. Commun.* 2160–2161 (2002) doi:10.1039/B205543K.
32. Zhou, Y., Sternlicht, H. & Padture, N. P. Transmission Electron Microscopy of Halide Perovskite Materials and Devices. *Joule* **3**, 641–661 (2019).
33. Suppressed phase segregation for triple-junction perovskite solar cells | Nature. https://www.nature.com/articles/s41586-023-06006-7.
34. Yang, Y. *et al.* Expanded Phase Distribution in Low Average Layer-Number 2D Perovskite Films: Toward Efficient Semitransparent Solar Cells. *Advanced Functional Materials* **31**, 2104868 (2021).
35. Barichello, J. *et al.* Semi-Transparent Blade-Coated FAPbBr3 Perovskite Solar Cells: A Scalable Low-Temperature Manufacturing Process under Ambient Condition. *Solar RRL* **7**, 2200739 (2023).

Acknowledgements

The authors acknowledge the "HY-NANO" project that received funding from the European Research Council (ERC) Starting Grant 2018 under the European Union's Horizon 2020 research and innovation program (Grant Agreement No. 802862, the Ministero dell'Università e della Ricerca (MUR) and the University of Pavia through the program "Dipartimenti di Eccellenza 2023-2027".

Author information

Corresponding Author

*Giulia Grancini – giulia.grancini@unipv.it

Department of Chemistry & INSTM, University of Pavia, Via T. Taramelli 14, 27100 Pavia, Italy

Authors

Andrea Zanetta - Università Degli Studi Di Pavia - Pavia (Italy), Department of Chemistry & INSTM, Via T. Taramelli 14, 27100 Pavia, Italy;

Badri Vishal - King Abdullah University of Science and Technology (KAUST), KAUST Solar Center (KSC), Physical Sciences and Engineering Division (PSE), Thuwal, 23955-6900, Kingdom of Saudi Arabia;

Fabiola Faini - Università Degli Studi Di Pavia - Pavia (Italy), Department of Chemistry & INSTM, Via T. Taramelli 14, 27100 Pavia, Italy;

Giovanni Pica - Università Degli Studi Di Pavia - Pavia (Italy), Department of Chemistry & INSTM, Via T. Taramelli 14, 27100 Pavia, Italy;

Sergio Marras - Center for Convergent Technologies, Istituto Italiano di Tecnologia, Via Morego 30, 16163 Genova, Italy;

Bumin Yildirim - King Abdullah University of Science and Technology (KAUST), KAUST Solar Center (KSC), Physical Sciences and Engineering Division (PSE), Thuwal, 23955-6900, Kingdom of Saudi Arabia;

Maxime Babics - King Abdullah University of Science and Technology (KAUST), KAUST Solar Center (KSC), Physical Sciences and Engineering Division (PSE), Thuwal, 23955-6900, Kingdom of Saudi Arabia;

Esma Ugur - King Abdullah University of Science and Technology (KAUST), KAUST Solar Center (KSC), Physical Sciences and Engineering Division (PSE), Thuwal, 23955-6900, Kingdom of Saudi Arabia;
Erkan Aydin - King Abdullah University of Science and Technology (KAUST), KAUST Solar Center (KSC), Physical Sciences and Engineering Division (PSE), Thuwal, 23955-6900, Kingdom of Saudi Arabia;
Stefaan De Wolf - King Abdullah University of Science and Technology (KAUST), KAUST Solar Center (KSC), Physical Sciences and Engineering Division (PSE), Thuwal, 23955-6900, Kingdom of Saudi Arabia;
Michele De Bastiani - Università Degli Studi Di Pavia - Pavia (Italy), Department of Chemistry & INSTM, Via T. Taramelli 14, 27100 Pavia, Italy.

Ethics declarations

The authors declare no competing interests.

Supplementary Files

This is a list of supplementary files associated with this preprint. Click to download.

- SolarCellsCheckList.pdf
- SupportingInformation.pdf